

## Antiferromagnetic fluctuations and the Hall effect of electron-doped cuprates: Possibility of a quantum phase transition at underdoping

S. Charpentier, G. Roberge, S. Godin-Proulx, X. Béchamp-Laganière, K. D. Truong, and P. Fournier\*  
*Canadian Institute for Advanced Research, Regroupement québécois sur les matériaux de pointe and Département de Physique,  
 Université de Sherbrooke, Sherbrooke, Québec, Canada J1K 2R1*

P. Rauwel

*Department of Ceramics and Glass Engineering, CICECO, Universidade de Aveiro, Campus Universitário de Santiago,  
 3810-193 Aveiro, Portugal*

(Received 11 December 2009; revised manuscript received 5 February 2010; published 9 March 2010)

We present a complete analysis of the temperature dependence of the Hall coefficient  $R_H(T)$  as a function of cerium doping,  $x$ , on improved thin films of  $\text{Pr}_{2-x}\text{Ce}_x\text{CuO}_{4\pm\delta}$  made by pulsed-laser deposition. By mapping its first temperature derivative  $dR_H(T)/dT$  in a temperature-doping phase diagram, we show that some of the most important variations of  $R_H(T,x)$  occur in a  $T$ - $x$  range just above the antiferromagnetic (AF) transition,  $T_N(x)$ . This area of large  $dR_H(T)/dT$  in the phase diagram collapses at underdoping, very close to the onset of superconductivity at  $x=0.12$ . Assuming that this zone remains above  $T_N(x)$ , it suggests the presence of a zero-temperature critical point at underdoping in the phase diagram of the electron-doped cuprates on top of the one reported at  $x^*\sim 0.165$ . Both of these critical points can be related to specific transitions in Fermi-surface morphology with doping observed by ARPES. Hence, we conclude that the phase diagram of the  $n$ -type family presents two zero-temperature critical points similar to the  $p$ -type cuprates, setting clear limiting boundaries for theoretical models, in particular, the absence of long-range AF order between  $x=0.12$  and  $x^*\sim 0.165$ .

DOI: [10.1103/PhysRevB.81.104509](https://doi.org/10.1103/PhysRevB.81.104509)

PACS number(s): 74.62.Dh, 74.72.-h

### I. INTRODUCTION

The Hall effect is a very sensitive probe of Fermi-surface reconstructions in strongly correlated electronic materials. For high-temperature superconducting cuprates, the progression with doping of the temperature dependence of the Hall coefficient,  $R_H$ , can reveal anomalies in the phase diagram arising from competing or coexisting phases and leading to such Fermi-surface reconstructions.<sup>1-7</sup>  $R_H(T)$  behaves also similarly in related electronic systems presenting, for example, charge-density waves<sup>8</sup> or magnetic field induced phase transitions (see, for example, Refs. 9 and 10). In some cases, the influence of these phases is the strongest in proximity to a quantum critical point (QCP), the ending point of a phase line at zero temperature where quantum fluctuations affect strongly several physical properties over an extended temperature (or field) range.<sup>9,10</sup> The Hall coefficient can even change sign as a function of temperature when approaching such a point in the phase diagram,<sup>1,2,4,8</sup> a clear indication that the Fermi surface can undergo major modifications, sometimes generating new carrier pockets in proximity to such transitions.

The electron-doped cuprates  $\text{Re}_{2-x}\text{Ce}_x\text{CuO}_{4\pm\delta}$  (Re=Pr, Nd, Sm) (Ref. 11) present such reconstruction of the Fermi surface evolving dramatically with doping. Angle-resolved photoemission spectroscopy (ARPES) reveals, in fact, a three-step process in the evolution of the Fermi surface in momentum space as the doping,  $x$ , is varied.<sup>12,13</sup> (1) a first set of Fermi arcs, close to  $\vec{k}=(0, \pi/a)$  (and equivalent points), appears at low doping with their length growing steadily with doping. It can be linked to the electronlike carriers observed by transport for underdoping ( $x < 0.15$ ).<sup>14-20</sup>

(2) Around optimal doping ( $x_{opt}\sim 0.15$ ), a second set of Fermi arcs close to  $\vec{k}=(\pi/2a, \pi/2a)$  adds to the electron arcs, both sets separated by the so-called hot spots.<sup>21,22</sup> These  $(\pi/2a, \pi/2a)$  arcs have been linked to the appearance of holelike carriers in transport.<sup>14-20</sup> (3) These  $(\pi/2a, \pi/2a)$  hole Fermi arcs merge eventually with the  $(0, \pi/a)$  electron arcs at overdoping ( $x \geq 0.17$ ) forming a large Fermi surface (cylinder) centered around  $\vec{k}=(\pi/a, \pi/a)$  (Ref. 13) similar to that observed in overdoped  $p$ -type cuprates.<sup>23,24</sup>

The doping dependence of the zero-temperature Hall coefficient of electron-doped cuprates<sup>11</sup> reveals an anomaly at overdoping ( $x^*\sim 0.165$ ) interpreted as the signature of a QCP hidden under the superconducting dome.<sup>25</sup> This special doping corresponds to the merging point of the above-mentioned hole and electron Fermi arcs as observed by ARPES.<sup>13</sup> Quantum oscillations in the magnetoresistance<sup>26</sup> suggest actually a transition from small electron and hole pockets for  $x < x^*$  to a large hole cylinder for  $x > x^*$ . Optical spectroscopy has confirmed that  $x^*\sim 0.165$  corresponds to the end of the pseudogap line,  $T^*(x)$ ,<sup>21,22</sup> a crossover temperature where substantial changes in spectral weight can be first detected, similar but not identical to the features observed in the  $p$ -type cuprates.<sup>27</sup> Relying on elastic neutron-scattering measurements showing substantial antiferromagnetic correlations up to  $x=0.17$ ,<sup>28</sup> the same QCP was also interpreted and used in a few theoretical approaches as the ending point of the long-range antiferromagnetic (Néel) order.<sup>19,20,29,30</sup> The resulting phase diagram suggests that superconductivity (SC) and antiferromagnetism (AF) coexist over a wide range of doping from  $0.12 < x < 0.165$  under the superconducting dome, i.e., up to overdoping, as illustrated in Fig. 1(a). The coexistence of SC and AF over such a large

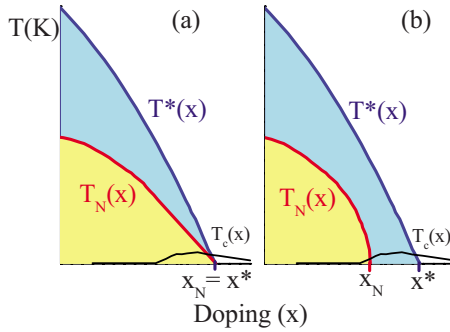


FIG. 1. (Color online) Schematics of the two competing scenarios for the phase diagram of electron-doped cuprates where the red and the blue solid lines are the  $T_N(x)$  and  $T^*(x)$  phase lines, respectively. (a)  $T_N(x)$  and  $T^*(x)$  are converging to a lone quantum critical point at  $x^* \sim 0.165$  implying long-range antiferromagnetic order up to this point as suggested by several experiments (Refs. 21, 22, 25, and 28); (b)  $T_N(x)$  is vanishing in the underdoped region of the phase diagram at a point that is distinct from  $x^*$  as was shown using inelastic neutron scattering (Ref. 33). The black solid line is  $T_c(x)$ . The scenario in (b) is similar to the observations for hole-doped cuprates.

range of doping would represent a very distinctive feature of the electron-doped cuprates with respect to their hole-doped cousins with their separate zero-temperature critical points as in Fig. 1(b).<sup>27,31,32</sup> Obviously, the confirmation of such scenario is likely to be decisive in our choice of an appropriate theoretical approach linking Fermi-surface reconstruction, antiferromagnetism and its corresponding fluctuations, and ultimately superconductivity.

Recently, Motoyama *et al.*<sup>33</sup> have interpreted the loss of spin stiffness and the related absence of a diverging correlation length in the  $0.134 < x < 0.165$  doping range from their inelastic neutron-scattering (INS) measurements on  $\text{Nd}_{2-x}\text{Ce}_x\text{CuO}_{4\pm\delta}$  (NCCO) single crystals as evidence that long-range AF order does not really persist up to  $x^* = 0.165$ . A second quantum critical point defined by the collapse of the  $T_N(x)$  line at  $x_N \sim 0.134$  is thus identified. Their results are in direct conflict with the above-mentioned reports as they seem to confirm instead a scenario similar to the hole-doped cuprates as in Fig. 1(b) with little, maybe even no coexistence of SC and AF. In this zone of interest for  $0.134 < x < 0.165$ , only short-range order and strong magnetic fluctuations remain while the superconducting transition temperature reaches its maximum value. In such scenario, the Hall effect should be sensitive to this transition.

Here, we present an analysis of the full temperature and doping dependence of the Hall coefficient,  $R_H(T, x)$ , of improved electron-doped cuprate thin films and demonstrate that it can be used to track  $T_N(x)$ . The largest variations of  $R_H$  are observed for temperatures and doping just above  $T_N(x)$ . The resulting phase diagram pinpoints to a zero-temperature antiferromagnetic phase transition at underdoping and ruling out the presence of antiferromagnetic long-range order beyond  $x \sim 0.125$  in  $\text{Pr}_{2-x}\text{Ce}_x\text{CuO}_{4\pm\delta}$  in accordance with the INS interpretation of Motoyama *et al.*<sup>33</sup>

## II. EXPERIMENTAL SETUP AND PROCEDURES

Epitaxial *c*-axis-oriented  $\text{Pr}_{2-x}\text{Ce}_x\text{CuO}_{4\pm\delta}$  (PCCO) thin films were grown by pulsed-laser deposition (PLD) follow-

ing a new procedure reported elsewhere.<sup>34</sup> This approach based on the addition of excess CuO in the targets improves significantly the quality of these films. In fact, it rids them of a parasitic intercalated and epitaxial phase identified as  $(\text{Pr,Ce})\text{O}_2$  (isostructural to  $\text{CeO}_2$ ) and related to the extended defects observed in large single crystals.<sup>35,36</sup> This situation arises mainly due to their difficult growth and post-annealing (reduction) conditions close to a decomposition line leading to phase competition. The appearance of such planar epitaxial intergrowths mainly composed of Cu-poor phases was even proposed to be a necessary product of the reduction process required to induce superconductivity.<sup>36</sup> In the old generation of thin films prepared by PLD, the parasitic phase is observed as an extra peak in the x-ray  $\theta$ - $2\theta$  diffraction patterns at  $2\theta \sim 32.3^\circ$  ( $\text{Cu } K\alpha$ ).<sup>37,38</sup> In Fig. 2(a), we show this x-ray diffraction pattern (top red solid line) in the vicinity of PCCO's (004) peak. A low-resolution transmission electron microscopy (TEM) image in Fig. 2(c) confirms the dramatic impact of the intercalated phases on the microstructure.<sup>34</sup>

After modifying the growth conditions with these off-stoichiometric PLD targets,<sup>34</sup> the parasitic phase vanishes completely in the x-ray pattern in Fig. 2(a) (blue solid line) resulting in uniform PCCO epitaxial films with very sharp interfaces with the substrates.<sup>34</sup> The impact of the improved microstructure is clearly observed in the absolute value of the in-plane resistivity as a function of temperature in Fig. 2(b). The new optimally doped thin films ( $x=0.15$ ) reach resistivity values close to  $25 \mu\Omega \text{ cm}$  just above  $T_c$ , very comparable to the best electron-doped thin films grown by molecular-beam epitaxy.<sup>15,39</sup> Even the magnitude of the Hall coefficient is affected by such improved microstructure as shown in Ref. 34 and will have a major impact on our following interpretation of the doping dependence of the zero-temperature  $R_H$  in comparison to a previous report.<sup>19,25</sup>

Several cerium contents were explored and as many as eighty (80) samples were measured. We focused mostly on the underdoped region ( $x < 0.15$ ) with eight different compositions between  $x=0.10$  and  $0.15$ . Since we cannot measure the amount of oxygen removed during the reduction process (an *in situ* vacuum postannealing of roughly 5 min), all the films showing superconductivity  $0.12 < x \leq 0.20$  were annealed in conditions maximizing the transition temperature ( $T_c$ ). For the nonsuperconducting underdoped films ( $x \leq 0.11$ ), we chose to anneal the films in the same conditions as the  $x=0.12$  films.

To evaluate the Hall coefficient of our films with great accuracy, we have measured their thicknesses using scanning electron microscopy at grazing incidence on freshly cleaved samples. Most of the samples had thicknesses of roughly 200–300 nm (with an uncertainty of less than 5 nm). The longitudinal resistivity and the Hall coefficient were measured in a physical properties measurement system (Quantum Design). The films were not patterned to avoid any major degradation from the usual lithographic processes. The Hall resistivity was evaluated at 9 T for all temperatures and its linear field dependence at fixed temperatures was also checked when required (for example, at low temperature when superconductivity is suppressed). We have also measured the resistivity in zero field and in a field of 9 T. This

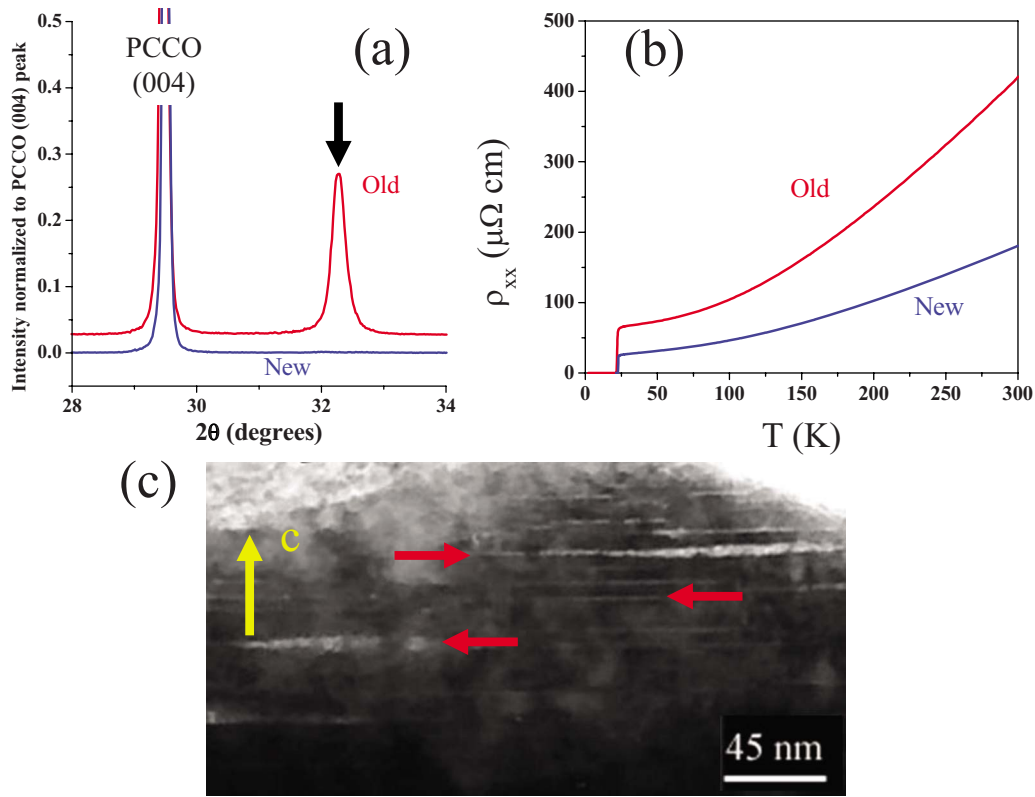


FIG. 2. (Color online) (a) X-ray diffraction patterns of PCCO thin films with  $x=0.15$  with the  $\theta$ - $2\theta$  technique using the Cu  $K\alpha$  radiation for the old generation thin films (red) and the new ones (blue) clearly showing the disappearance of the parasitic phases. The red curve is shifted upward for clarity. (b) In-plane resistivity as a function of temperature for the old (red) and new (blue) generations of films for  $x=0.15$ . (c) Low-resolution cross-sectional TEM image of an old generation thin film for  $x=0.15$ . The dark material is PCCO while the arrows point to the intercalated epitaxial phase (light gray). The yellow arrow points along the  $c$ -axis direction.

large field is sufficient to suppress completely superconductivity, except for  $x=0.135$  and  $0.14$ .

### III. RESULTS AND DISCUSSION

#### A. Doping and temperature dependence of transport properties

In Fig. 3, we show the resistivity data of the films for selected cerium concentrations. First, we observe that the doping dependence of the low-temperature resistivity (at 2 K) is strong at low doping as it changes by an order of magnitude up to  $x\sim 0.13$ , while it flattens out beyond optimal doping. We can also observe that the temperature corresponding to the minimum in resistivity decreases with increasing doping reaching a zero value very close to that observed previously at  $x\sim 0.165$  (Ref. 16) (see below). Except for the absolute value of the resistivity, the overall trends observed previously in PLD films are preserved in the new generation of thin films.

In Fig. 4(a), we present a complete set of the measured Hall coefficient as a function of temperature for all the composition values studied.<sup>40</sup> From these data, one can first extract the doping dependence of the zero-temperature Hall coefficient (our data is limited to the values at 2 K). In Fig. 5(a) we compare our results of the absolute value of the Hall coefficient in our improved thin films to those reported pre-

viously in Ref. 25 and in Fig. 2 of Ref. 17. As mentioned above, the removal of the parasitic phase rescales the magnitude of the Hall coefficient at low temperature. Despite this change in the absolute value, the same anomalies at  $x\sim 0.11$  and  $x\sim 0.165$  can be observed in both data sets. In Fig. 6, we present the resistivity of an  $x=0.17$  PCCO thin film. We can observe that the low-temperature resistivity

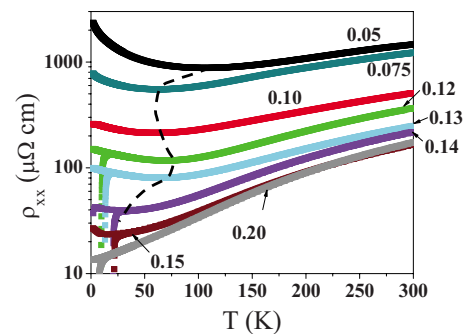


FIG. 3. (Color online) In-plane resistivity  $\rho_{xx}$  as a function of temperature at zero applied magnetic field and at 9 T down to 2 K for selected Ce contents showing the strong decrease in  $\rho_{xx}$  at 2 K for low doping (for  $x < 0.13$ ) compared to that at high doping ( $x > 0.13$ ). Note that the vertical axis is on a logarithmic scale. The black dashed line tracks the temperature corresponding to the minimum in resistivity and its doping dependence (see text).

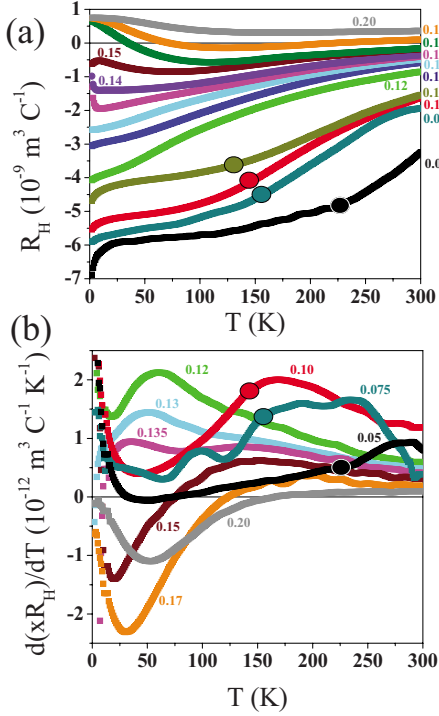


FIG. 4. (Color online) (a) The Hall coefficient as a function of temperature for cerium contents ranging from  $x=0.05$  (bottom in black) to  $x=0.20$  (top in gray). The circles indicate the Néel temperature as measured by elastic neutron scattering. (b) The first derivative of the Hall coefficient as a function of temperature for selected cerium contents ranging from  $x=0.05$  (in black) to  $x=0.20$  (in gray). In here, the color coding between panels (a) and (b) is preserved.

reaches values as low as  $15 \mu\Omega \text{ cm}$ , but most importantly, it is completely linear down to 340 mK, reproducing the trend observed in Ref. 16 and identifying the intergrowths as the source of the apparent upturns observed by Dagan *et al.*<sup>25</sup> even for  $x=0.17$ . We conclude, as was done in Ref. 25, that the anomaly at  $x \sim 0.165$  in  $R_H(x)$  in Fig. 5(a) and the linear resistivity down to the lowest temperature in Fig. 6 reveal all the trends of a material in proximity to a quantum critical point at  $x^* \sim 0.165$ .

Our data for  $x \geq 0.10$  follows closely a calculation by Lin and Millis<sup>19,20</sup> shown as a green dashed line in Fig. 5(a). This result assumes the existence of long-range antiferromagnetism up to  $x^* \sim 0.165$  and relying on spin-density waves (SDW) to generate the Fermi-surface reconstructions observed by ARPES.<sup>12,13</sup> Such mechanism leads to a transformation of the large hole Fermi surface centered at  $\vec{k}=(\pi/a, \pi/a)$  due to the opening of a (pseudo) gap in the vicinity of the antiferromagnetic Brillouin zone boundaries. As underlined by Lin and Millis,<sup>19</sup> the absolute value of the measured  $R_H(x)$  at  $T=0$  for the old generation of films was too large in the underdoped regime ( $0.11 < x < 0.15$ ) and did not follow also the doping dependence in the overdoped regime ( $x > 0.17$ ). The removal of the intergrowths solved essentially both problems.

We should insist here on the fact that, contrary to the previous data obtained with the old generation of films,<sup>19,25</sup>

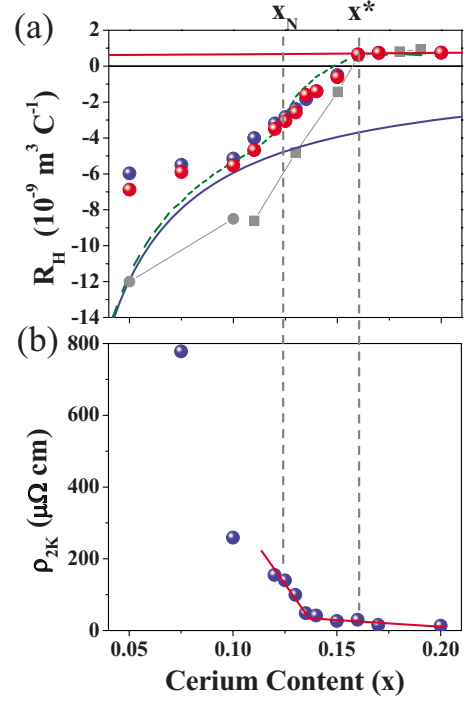


FIG. 5. (Color online) (a) Low-temperature Hall coefficient as a function of doping showing the anomalies at  $x \sim 0.10$  and  $x \sim 0.165$ . Blue circles: approximate Hall coefficient on the plateau. Red circles: Hall coefficient at 2 K. Gray squares: absolute values on the old generation of films (Ref. 25). Gray circles: our results for  $x=0.05$  and  $0.10$  on similar films (Ref. 17). Solid blue line:  $R_H = -V_{UC}(x)/2xe$ . Solid red line:  $R_H = V_{UC}(x)/2(1-x)e$ . Dashed green line: theoretical prediction from Lin and Millis (Ref. 19) based on the SDW model. (b) Resistivity at 2 K and 9 T as a function of doping (red solid lines are guides to the eyes) extracted from the resistivity data from Fig. 3 for several cerium contents.

the absolute value of  $R_H$  at all temperatures always lies between the two boundaries set by the expected low-temperature limiting carrier concentrations controlled by doping and the corresponding volume encompassed by the Fermi surface (pockets, arcs, large cylinder).<sup>19</sup> For low doping, a small electron pocket (arcs) with a total volume in  $k$  space proportional to  $x$  should give  $R_H = -V_{UC}(x)/2xe$  [blue solid line in Fig. 5(a)]. For  $x > x^*$ , a large hole Fermi surface

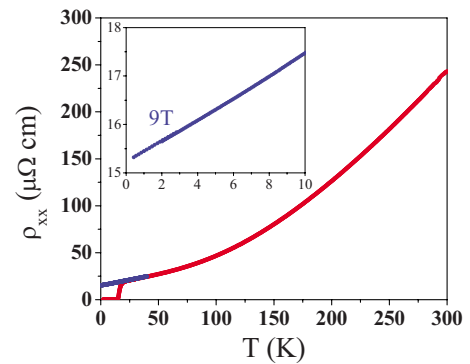


FIG. 6. (Color online) In-plane resistivity as a function of temperature for  $x=0.17$ . Red data are at 0 T while the blue ones are at 9 T. Inset: the low-temperature dependence down to 340 mK.

centered at  $\vec{k}=(0, \pi/a)$  with a total volume proportional to  $1-x$  should result in  $R_H=V_{UC}(x)/2(1-x)e$  [red solid line in Fig. 5(a)]. Here,  $V_{UC}\sim 0.190\text{ nm}^3$  is the volume of the unit cell taking into account PCCO's decreasing  $c$ -axis lattice parameter with increasing Ce doping in thin films<sup>41</sup> while a factor of 2 is used since there are actually two copper atoms per unit cell (it contains two formula units).

It is also tempting to link the anomaly in  $R_H(x)$  at  $x\sim 0.10$  in Fig. 5(a) to another quantum phase transition expected if the AF long-range order vanishes at underdoping as demonstrated by Motoyama *et al.*<sup>33</sup> However, we must underline a significant discrepancy between the theoretical values (solid blue and dashed green lines) and the measured low-temperature  $R_H$  for  $x=0.05$  and  $0.075$  in Fig. 5(a). Since the reduction process is known to result in the largest changes in oxygen content for low cerium doping<sup>42,43</sup> and that we are relying on the annealing conditions of the  $x=0.12$  sample to reduce the nonsuperconducting samples for  $x<0.12$ , one cannot rule out the possibility that the  $R_H$  absolute values deviate from theory for these low cerium contents as a result of a significant extra electron doping because of excess reduction. The kink at  $x\sim 0.10$  would then be an artifact. Moreover, as shown in Fig. 5(b), the doping dependence of the low-temperature resistivity shows also a sudden change in behavior at underdoping,  $x\sim 0.135$ , and not at  $x^*\sim 0.165$ . It clearly shows that the change in topology of the Fermi surface at  $x^*\sim 0.165$  revealed using  $R_H$  is not accompanied by a substantial change in the doping dependence of  $\rho_{xx}$ . It suggests also that the onset of an additional source of scattering occurs as one decreases  $x$  away from  $x^*$ . Since the observed anomalies in  $R_H$  and  $\rho_{xx}$  at underdoping do not occur exactly at the same doping, we cannot rely on the zero-temperature data to identify the presence of a QCP linked to the suppression of long-range AF order. In what follows, we try to extract such information from the  $R_H$  data at finite temperature.

## B. Finite-temperature $R_H$ and derivative mapping

An interesting feature in Fig. 4(a) is the relative flatness of  $R_H(T)$  for  $x=0.05$  in the 0–200 K temperature range. In fact, the related kneelike anomaly marking the crossover from the low- to high-temperature regimes can also be observed for  $x=0.075, 0.10, 0.11$ , and even  $0.12$ . For  $x=0.05, 0.075$ , and  $0.10$ , these corresponding crossover temperatures coincide closely to the Néel temperature estimated from elastic neutron-scattering measurements on NCCO single crystals<sup>28</sup> and shown as large circles in Fig. 4(a). It suggests that the origin of the plateau-like behavior of the Hall coefficient is related to the onset of long-range antiferromagnetic order. Except for the lowest temperatures, the charge-carrier density extracted from the Hall coefficient tends to a constant below the Néel temperature for these dopings, which may indicate that the Fermi-surface reconstruction stops or that its trend is modified as the temperature crosses  $T_N$  for a given  $x$  value. This plateau(knee)like behavior disappears at a doping close to  $x=0.12$ . Of course, such link of  $R_H$  to  $T_N$  should be observable by ARPES. For example, with  $x=0.05$ , the Fermi-surface reconstruction should be visible as one de-

creases the temperature from  $T^*$  to  $T_N$  as a gradual change in the spectral weight around the hot spots. At this point, our data suggest that this hot-spot spectral weight should stop evolving for  $T<T_N$ . We expect also optical spectroscopy to present a related anomaly.

We should underline here that an anomaly in the Hall effect at the Néel temperature has already been observed in a simple system like chromium (Cr) where the carrier density presents a fairly steep change at the transition.<sup>44</sup> Interestingly, the transition corresponds also to a change from a temperature-dependent  $R_H$  above  $T_N$  to an almost temperature-independent one at low enough temperature away from  $T_N$ . This behavior was interpreted theoretically by Norman *et al.*<sup>45</sup> as a signature of nesting in an itinerant antiferromagnet in the vicinity of a quantum critical point. In this particular case, the nesting leads to a sudden removal of portions of the Fermi surface of Cr upon entering the magnetic order. The change in the Fermi surface in Cr occurs obviously at temperatures very close to  $T_N$  (within a few kelvin at most) as the fluctuation regime of this three-dimensional antiferromagnet is likely quite narrow in temperature. In the case of electron-doped cuprates, as one fixes the doping, say to  $x=0.10$ , and decreases the temperature from  $T>T^*$ , the Fermi surface removal starts at  $T^*$  and stops at  $T_N$ , a temperature range where significant antiferromagnetic correlations are observed by INS.<sup>33</sup> Thus, there is a wide range of temperature where the Hall coefficient increases negatively that could be linked to a gradual evolution of the Fermi-surface topology.

Another distinctive signature in Fig. 4(a) is the gradual growth of a positive upturn in  $R_H(T)$  at low temperatures for doping above  $x\sim 0.14$ . This feature has been interpreted as the first sign of holelike carriers in transport<sup>14–18</sup> and coincides with the onset of superconductivity in the phase diagram.<sup>18</sup> One of its most notable impacts in the data is the observation of a minimum in  $R_H(T)$  for  $x\geq 0.15$ . Interestingly, this minimum appears at an increasing temperature with increasing Ce concentration even for the most overdoped films. At  $x=0.20$ ,  $R_H$  still presents a temperature dependence that cannot really be explained by a simple single-band Fermi-liquid picture with isotropic scattering rate even though the Fermi surface does not seem to present any traces of the hot spots from ARPES.<sup>13</sup> A thorough analysis of angular magnetoresistance oscillations to extract the anisotropy of the scattering rate<sup>3</sup> may provide important clues to clarify the origin of this temperature dependence of  $R_H$ . We should mention that recent ac Hall angle studies of the same PCCO thin films<sup>46,47</sup> propose that current vertex corrections from AF fluctuations may explain qualitatively several of the features in their dc and ac Hall effect.

Overall, for both low and high Ce concentrations, these special features in  $R_H(T)$  correspond to significant changes in the slope (i.e., in  $dR_H/dT$ ). It suggests using the first derivative of  $R_H(T)$  with respect to temperature to track the probable signatures of the Néel transition and the crossover from electron- to hole-dominated transport and map them as a function of doping.

In Fig. 4(b), we present the temperature dependence of this first derivative,  $d(xR_H)/dT$ , for several Ce concentrations. For clarity, we have removed a few curves and multi-

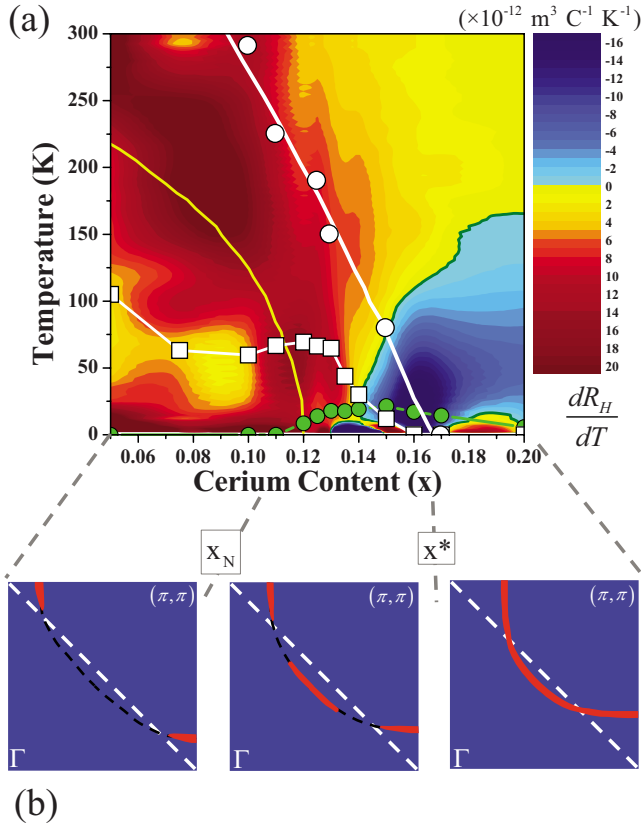


FIG. 7. (Color online) (a) Contour plot showing the mapping of  $dR_H/dT$  as a function of temperature and doping. The yellow solid line is a rough schematic of the expected  $T_N(x)$  line. The white circles are extracted from Refs. 21 and 22 and represent the pseudogap  $T^*(x)$  line (the white line is a guide to the eyes). The green circles show the superconducting  $T_c(x)$  phase line. The bold green line corresponds to  $dR_H/dT=0$ . (b) Schematics of the Fermi surface observed in ARPES intensity integrated around the Fermi energy for  $x < x_N$  (left),  $x_N < x < x^*$  (center), and  $x > x^*$  (right).

plied the  $R_H(T)$  data by the corresponding Ce content,  $x$ , in order to magnify the relatively low derivative obtained for high values of  $x$ . As expected, this derivative reveals the presence of substantial changes in the temperature dependence of  $R_H(T)$ . For temperatures just above the plateaulike feature observed in  $R_H(T)$  for the low Ce contents, a clear maximum in the derivative corresponding to the inflexion point in  $R_H(T)$  can be tracked as a function of Ce content. For  $x=0.05$ ,  $0.075$  (not shown), and  $0.10$ , this maximum occurs at a temperature slightly above the Néel temperature as determined by neutron scattering and indicated by the large circles in Fig. 4(b). This maximum moves to and vanishes at low temperatures as the Ce doping reaches  $x \sim 0.13$ . For high Ce contents (above  $x=0.14$ ), the derivative shows another broad maximum developing at high temperatures followed by a sign change at low temperatures, both signaling the emergence of dominant holelike electrical transport in this range of temperatures and doping.

In order to draw a clearer picture from the information available from this derivative, we present a contour plot in the  $T$ - $x$  plane from our whole data set in Fig. 7(a). It reveals immediately the presence of a dominant maximum (the dark

red area) in  $dR_H/dT$  mimicking the expected temperature dependence of the phase line separating the Néel and the paramagnetic phases. This large positive derivative zone is converging at underdoping to  $x \sim 0.125$  and extends all the way to  $T^*(x)$  (obtained by optical spectroscopy<sup>21,22</sup>) shown in Fig. 7(a) as white circles. As mentioned above, the corresponding inflexion points in  $R_H(T)$  are above  $T_N(x)$ , at least for  $x=0.05$ ,  $0.075$ , and  $0.10$  according to neutron scattering. Assuming that these inflexion points remain above  $T_N(x)$  for  $x > 0.10$ , such analysis of the temperature and doping dependence of the Hall effect suggests that the maximum derivative corresponding to the largest changes in  $R_H$  with temperature and doping coincides with the region of the phase diagram where AF fluctuations are the strongest, i.e., for  $T \geq T_N(x)$  as signaled by the divergence of the correlation length observed in Ref. 33 using INS. Most importantly, our approach would be confirming the result of Motoyama *et al.*<sup>33</sup> that  $T_N(x)$  goes to zero at underdoping for  $x=x_N \sim 0.125$  in PCCO. The exact  $x$  value corresponding to this collapse of the maximum derivative remains ill defined due, in particular, to the additional features observed at low temperature in  $R_H(T)$ . The nature of the paramagnetic region where  $dR_H/dT$  is the largest is obviously of great interest since it corresponds to the regime where superconductivity reaches its maximum transition temperature and where the Hall effect presents the largest changes as a function of temperature and doping.

In this mapping, we can also notice the signature of the holelike contribution to the Hall coefficient (in blue). It is dominant at low temperature in a region of the phase diagram starting approximately at  $x \sim 0.135$  and extending to the whole overdoped region. Very interestingly, the large region with negative  $dR_H/dT$  includes most of the superconducting dome. As was proposed in many previous reports,<sup>14–18</sup> these signatures of holelike carriers coinciding with the presence of superconductivity strongly suggest that the hole arcs located close to  $\vec{k}=(\pi/2a, \pi/2a)$  as illustrated in the middle panel of Fig. 7(b) are required to induce superconductivity. This point of view is also consistent with ARPES results showing the disappearance of the same hole arcs in nonsuperconducting as-grown PCCO single crystals when compared to the superconducting reduced ones.<sup>48</sup> Moreover, the derivative mapping emphasizes the presence of the QCP at  $x^*=0.165$  in the phase diagram and its impact on the transport properties as a region with the strongest negative  $dR_H/dT$  [dark blue region of Fig. 7(a)]. In general,  $T^*(x)$  away from this QCP is hardly visible from in-plane transport properties: it has been clearly observed though in  $c$ -axis resistivity,<sup>49</sup> a component difficult to access using thin films.

Another interesting feature observed with our numerous doping values explored between  $x=0.05$  and  $0.15$  is the presence of an anomaly in the doping dependence of the temperature corresponding to a minimum in resistivity illustrated in Fig. 3 (dashed line) and defined as  $T_{min}$ . This minimum was previously tracked at a so-called metal-insulator transition at  $x^*$ .<sup>50</sup> In our thin films, the trend is preserved as shown in Fig. 7(a), but an anomaly is observed at  $x \sim 0.125$  as  $T_{min}(x)$  crosses the region where  $dR_H/dT$  reaches its maximum value. Since we attributed these large variations of

$dR_H/dT$  to the presence of AF fluctuations, this anomaly is likely an indication that additional scattering by AF fluctuations contribute to resistivity in this particular part of the phase diagram. It is likely the same source of additional scattering that causes the above-mentioned sudden change of resistivity in Fig. 5(b) at  $x \sim 0.135$ .

Our results summarized in Fig. 7(a) support a universal phase diagram for hole and electron doping in the cuprates with the  $T_N(x)$  and  $T^*(x)$  phase lines vanishing at two different zero-temperature points as shown in Fig. 1(b). However, contrary to the hole-doped cuprates, the collapse of long-range antiferromagnetic order at  $x_N$  leads to a transition from a single electron Fermi arc close to  $\vec{k}=(0, \pi/a)$  to a combination of electron and hole arcs above (or away from)  $T_N(x)$  as illustrated in Fig. 7(b). In this region, the AF fluctuations are the strongest and of course, the reconstruction coincides closely with the onset of superconductivity. As was recently suggested by Sachdev,<sup>51</sup> the region located between  $x_N$  and  $x^*$  is likely dominated by short-range AF order that continues to contribute to the reconstruction. Beyond  $x^*$ , a single Fermi surface is recovered as shown by Matsui *et al.*<sup>13</sup>

Assuming that the dark red regions in Fig. 7(a) are close to the  $T_N(x)$  line all the way to a zero-temperature (quantum) critical point, we cannot rule out the possible coexistence of superconductivity and long-range antiferromagnetism as was underlined previously from INS on NCCO.<sup>33</sup> However, if there is such coexistence, it is limited to a very small doping range from  $x=0.11$  to  $0.13$  in the underdoped regime for PCCO as underlined by Motoyama *et al.*,<sup>33</sup> and would surely not extend to  $x^*$ . One should note that the slight difference in  $x_N$  between PCCO and NCCO may be related to the coupling of the Nd magnetic moments to the Cu ones (see Ref. 52 and references therein) strengthening slightly spin stiffness in NCCO with respect to PCCO. Moreover, the impact of different reduction processes and even strain-induced effects may also explain this difference in  $x_N$  between PCCO thin films and NCCO crystals. Nevertheless, the major conclusion that  $x_N$  is on the underdoped side of the  $T_c(x)$  superconducting dome is confirmed in both systems using very different probes. Obviously, a similar study with NCCO thin films may help clarifying the origin of the small disagreement.

Finally, we need to comment on the possibility of similar signatures in the Hall effect of hole-doped cuprates. Relying on recent data on single crystals<sup>53,54</sup> of  $\text{La}_{2-x}\text{Sr}_x\text{CuO}_4$  (LSCO), one can actually observe intervals of temperature

below roughly 300 K where  $R_H(T)$  is relatively flat for a doping ranging from  $x=0.01$  to  $0.05$ . This area in the phase diagram where  $dR_H/dT$  is close to zero corresponds also to a region where the Néel temperature collapses to zero at  $x \sim 0.03$ . These signatures may be related to our observations, although their manifestation are not as well defined as that of the electron-doped cuprates due to the limited region of the phase diagram where the antiferromagnetic phase persists. The difference may also be due to a different impact of the antiferromagnetic order and its fluctuations on the Fermi-surface reconstruction in the hole-doped cuprates, which occur far away from the nodal points at  $(\pi/2a, \pi/2a)$  contrary to the electron-doped cuprates. Moreover, the large  $dR_H/dT$  at large temperature (above room temperature) in LSCO was also interpreted quite differently as a manifestation of strong charge fluctuations over a gap.<sup>54</sup> It is interesting also to note that similar features have been observed in  $\text{YBa}_2\text{Cu}_3\text{O}_7$  (Ref. 55) and Bi-based cuprate single crystals.<sup>56</sup> It would be interesting to focus further on these two families since they both present an extended doping range in the phase diagram with long-range antiferromagnetic order.

In summary, we have presented an alternate route to analyze the temperature dependence of the Hall coefficient of electron-doped high-temperature superconductors. We have focused mainly in the evolution of anomalies in its temperature derivative observed as the cerium doping is varied. The zone of the phase diagram where the derivative reaches its largest values tracks closely the phase line  $T_N(x)$  corresponding to the Néel transition. We show that this line vanishes at a zero-temperature (quantum) critical point at underdoping  $x \sim 0.125$ . This observation is consistent with a recent proposal based on inelastic neutron-scattering measurements on  $\text{Nd}_{2-x}\text{Ce}_x\text{CuO}_4$  single crystals and we propose that this point must be related to the Fermi-surface reconstruction observed by ARPES at underdoping.

#### ACKNOWLEDGMENTS

We thank A.-M. Tremblay, C. Bourbonnais, M. Poirier, S. Jandl, P. Richard, R. L. Greene, M. P. Singh, and L. Taillefer for discussions, S. Pelletier for his technical assistance, and J. Beerens for the thickness measurements. We acknowledge the support of the Canadian Institute for Advanced Research and funding from NSERC, FQRNT, and CFI. One of us (P.R.) acknowledges the financial support of CICECO.

\*patrick.fournier@usherbrooke.ca

<sup>1</sup>D. LeBoeuf, N. Doiron-Leyraud, J. Levallois, R. Daou, J.-B. Bonnemaison, N. E. Hussey, L. Balicas, B. J. Ramshaw, R. Liang, D. A. Bonn, W. N. Hardy, S. Adachi, C. Proust, and L. Taillefer, *Nature (London)* **450**, 533 (2007).

<sup>2</sup>F. F. Balakirev, J. B. Betts, A. Migliori, I. Tsukada, Y. Ando, and G. S. Boebinger, *Phys. Rev. Lett.* **102**, 017004 (2009).

<sup>3</sup>N. E. Hussey, *J. Phys.: Condens. Matter* **20**, 123201 (2008).

<sup>4</sup>N. Doiron-Leyraud, C. Proust, D. LeBoeuf, J. Levallois, J.-B. Bonnemaison, R. Liang, D. A. Bonn, W. N. Hardy, and L.

Taillefer, *Nature (London)* **447**, 565 (2007).

<sup>5</sup>C. Jaudet, D. Vignolles, A. Audouard, J. Levallois, D. LeBoeuf, N. Doiron-Leyraud, B. Vignolle, M. Nardone, A. Zitouni, R. Liang, D. A. Bonn, W. N. Hardy, L. Taillefer, and C. Proust, *Phys. Rev. Lett.* **100**, 187005 (2008).

<sup>6</sup>E. A. Yelland, J. Singleton, C. H. Mielke, N. Harrison, F. F. Balakirev, B. Dabrowski, and J. R. Cooper, *Phys. Rev. Lett.* **100**, 047003 (2008).

<sup>7</sup>L. Taillefer, *J. Phys.: Condens. Matter* **21**, 164212 (2009).

<sup>8</sup>R. Bel, K. Behnia, and H. Berger, *Phys. Rev. Lett.* **91**, 066602

- (2003).
- <sup>9</sup>S. Paschen, T. Luhmann, S. Wirth, P. Gegenwart, O. Trovarelli, C. Geibel, F. Steglich, P. Coleman, and Q. Si, *Nature (London)* **432**, 881 (2004).
- <sup>10</sup>M. A. Tanatar, J. Paglione, C. Petrovic, and L. Taillefer, *Science* **316**, 1320 (2007).
- <sup>11</sup>N. P. Armitage, P. Fournier, and R. L. Greene, arXiv:0906.2931 (unpublished).
- <sup>12</sup>N. P. Armitage, F. Ronning, D. H. Lu, C. Kim, A. Damascelli, K. M. Shen, D. L. Feng, H. Eisaki, Z.-X. Shen, P. K. Mang, N. Kaneko, M. Greven, Y. Onose, Y. Taguchi, and Y. Tokura, *Phys. Rev. Lett.* **88**, 257001 (2002).
- <sup>13</sup>H. Matsui, T. Takahashi, T. Sato, K. Terashima, H. Ding, T. Uefuji, and K. Yamada, *Phys. Rev. B* **75**, 224514 (2007).
- <sup>14</sup>P. Fournier, X. Jiang, W. Jiang, S. N. Mao, T. Venkatesan, C. J. Lobb, and R. L. Greene, *Phys. Rev. B* **56**, 14149 (1997).
- <sup>15</sup>F. Gollnik and M. Naito, *Phys. Rev. B* **58**, 11734 (1998).
- <sup>16</sup>P. Fournier, P. Mohanty, E. Maiser, S. Darzens, T. Venkatesan, C. J. Lobb, G. Czjzek, R. A. Webb, and R. L. Greene, *Phys. Rev. Lett.* **81**, 4720 (1998).
- <sup>17</sup>J. Gauthier, S. Gagné, J. Renaud, M.-E. Gosselin, P. Fournier, and P. Richard, *Phys. Rev. B* **75**, 024424 (2007).
- <sup>18</sup>Y. Dagan and R. L. Greene, *Phys. Rev. B* **76**, 024506 (2007).
- <sup>19</sup>J. Lin and A. J. Millis, *Phys. Rev. B* **72**, 214506 (2005).
- <sup>20</sup>A. J. Millis, A. Zimmers, R. P. S. M. Lobo, N. Bontemps, and C. C. Homes, *Phys. Rev. B* **72**, 224517 (2005).
- <sup>21</sup>Y. Onose, Y. Taguchi, K. Ishizaka, and Y. Tokura, *Phys. Rev. Lett.* **87**, 217001 (2001).
- <sup>22</sup>A. Zimmers, J. M. Tomczak, R. P. S. M. Lobo, N. Bontemps, C. P. Hill, M. C. Barr, Y. Dagan, R. L. Greene, A. J. Millis, and C. C. Homes, *Europhys. Lett.* **70**, 225 (2005).
- <sup>23</sup>M. Platé, J. D. F. Mottershead, I. S. Elfimov, D. C. Peets, R. Liang, D. A. Bonn, W. N. Hardy, S. Chiuzaibaian, M. Falub, M. Shi, L. Patthey, and A. Damascelli, *Phys. Rev. Lett.* **95**, 077001 (2005).
- <sup>24</sup>J. G. Analytis, M. Abdel-Jawad, L. Balicas, M. M. J. French, and N. E. Hussey, *Phys. Rev. B* **76**, 104523 (2007).
- <sup>25</sup>Y. Dagan, M. M. Qazilbash, C. P. Hill, V. N. Kulkarni, and R. L. Greene, *Phys. Rev. Lett.* **92**, 167001 (2004).
- <sup>26</sup>T. Helm, M. V. Kartsovnik, M. Bartkowiak, N. Bittner, M. Lambacher, A. Erb, J. Wosnitza, and R. Gross, *Phys. Rev. Lett.* **103**, 157002 (2009).
- <sup>27</sup>T. Timusk and B. Statt, *Rep. Prog. Phys.* **62**, 61 (1999).
- <sup>28</sup>P. K. Mang, O. P. Vajk, A. Arvanitaki, J. W. Lynn, and M. Greven, *Phys. Rev. Lett.* **93**, 027002 (2004).
- <sup>29</sup>X.-Z. Yan, Q. Yuan, and C. S. Ting, *Phys. Rev. B* **74**, 214521 (2006).
- <sup>30</sup>R. S. Markiewicz, *Phys. Rev. B* **70**, 174518 (2004).
- <sup>31</sup>D. M. Broun, *Nat. Phys.* **4**, 170 (2008).
- <sup>32</sup>J. L. Tallon and J. W. Loram, *Physica C* **349**, 53 (2001).
- <sup>33</sup>E. M. Motoyama, G. Yu, I. M. Vishik, O. P. Vajk, P. K. Mang, and M. Greven, *Nature (London)* **445**, 186 (2007).
- <sup>34</sup>G. Roberge, S. Charpentier, S. Godin-Proulx, P. Rauwel, K. Truong, and P. Fournier, *J. Cryst. Growth* **311**, 1340 (2009).
- <sup>35</sup>P. K. Mang, S. Larochelle, A. Mehta, O. P. Vajk, A. S. Erickson, L. Lu, W. J. L. Buyers, A. F. Marshall, K. Prokes, and M. Greven, *Phys. Rev. B* **70**, 094507 (2004).
- <sup>36</sup>H. J. Kang, P. Dai, B. J. Campbell, P. J. Chupas, S. Rosenkranz, P. L. Lee, Q. Huang, S. Li, S. Komiya, and Y. Ando, *Nature Mater.* **6**, 224 (2007).
- <sup>37</sup>E. Maiser, W. Mexner, R. Schafer, T. Schreiner, P. Adelman, G. Czjzek, J. L. Peng, and R. L. Greene, *Phys. Rev. B* **56**, 12961 (1997).
- <sup>38</sup>A. Lanfredi, S. Sergeenkov, and F. Araujo-Moreira, *Physica C* **450**, 40 (2006).
- <sup>39</sup>M. Naito, S. Karimoto, and A. Tsukada, *Supercond. Sci. Technol.* **15**, 1663 (2002).
- <sup>40</sup>At low temperature, one can clearly see traces of superconductivity not suppressed by the 9 T magnetic field for  $x=0.135$  and 0.14. This leads to a strong negative contribution to  $dR_H/dT$  that one can identify in the mapping of Fig. 7(a) under the superconducting dome. Since we are focusing on the normal-state properties in high magnetic field at finite temperature, we do not insist on this part of the data as it has no major impact on the interpretation.
- <sup>41</sup>E. Maiser, P. Fournier, J.-L. Peng, F. M. Araujo-Moreira, T. Venkatesan, R. Greene, and G. Czjzek, *Physica C* **297**, 15 (1998).
- <sup>42</sup>K. Suzuki, K. Kishio, T. Hasegawa, and K. Kitazawa, *Physica C* **166**, 357 (1990).
- <sup>43</sup>E. Navarro, D. Jaque, J. Villegas, J. Martyn, A. Serquis, F. Prado, A. Caneiro, and J. Vicent, *J. Alloys Compd.* **323-324**, 580 (2001).
- <sup>44</sup>A. Yeh, Y.-A. Soh, J. Brooke, G. Aeppli, T. F. Rosenbaum, and S. M. Hayden, *Nature (London)* **419**, 459 (2002).
- <sup>45</sup>M. R. Norman, Q. Si, Y. B. Bazaliy, and R. Ramazashvili, *Phys. Rev. Lett.* **90**, 116601 (2003).
- <sup>46</sup>G. S. Jenkins, D. C. Schmadel, P. L. Bach, R. L. Greene, X. Béchamp-Laganière, G. Roberge, P. Fournier, and H. D. Drew, *Phys. Rev. B* **79**, 224525 (2009).
- <sup>47</sup>G. S. Jenkins, D. C. Schmadel, P. L. Bach, R. L. Greene, X. Béchamp-Laganière, G. Roberge, P. Fournier, H. Kontani, and H. D. Drew, *Phys. Rev. B* **81**, 024508 (2010).
- <sup>48</sup>P. Richard, M. Neupane, Y.-M. Xu, P. Fournier, S. Li, P. Dai, Z. Wang, and H. Ding, *Phys. Rev. Lett.* **99**, 157002 (2007).
- <sup>49</sup>Y. Onose, Y. Taguchi, K. Ishizaka, and Y. Tokura, *Phys. Rev. B* **69**, 024504 (2004).
- <sup>50</sup>P. Fournier, E. Maiser, and R. L. Greene, in *The Gap Symmetry and Fluctuations in High- $T_c$  Superconductors*, NATO ASI Series B, edited by J. Bok, G. Deutscher, D. Pavuna, and S. Wolf (Plenum Press, New York, 1998), Vol. 371, p. 145.
- <sup>51</sup>S. Sachdev, arXiv:0907.0008 (unpublished).
- <sup>52</sup>P. Richard, M. Poirier, and S. Jandl, *Phys. Rev. B* **71**, 144425 (2005).
- <sup>53</sup>Y. Ando, Y. Kurita, S. Komiya, S. Ono, and K. Segawa, *Phys. Rev. Lett.* **92**, 197001 (2004).
- <sup>54</sup>S. Ono, S. Komiya, and Y. Ando, *Phys. Rev. B* **75**, 024515 (2007).
- <sup>55</sup>K. Segawa and Y. Ando, *Phys. Rev. B* **69**, 104521 (2004).
- <sup>56</sup>Y. Ando, Y. Hanaki, S. Ono, T. Murayama, K. Segawa, N. Miyamoto, and S. Komiya, *Phys. Rev. B* **61**, R14956 (2000).